Investigating the Thermal Stability of Highly Radiative Discharges on JET with a new Tomographic Method

by A.Murari[1,2], E.Peluso[2] , T.Craciunescu[3], C.Lowry[4], S.Aleiferis[5], P.Carvalho[5], M.Gelfusa[3] and JET Contributors*

EUROfusion Consortium, JET, Culham Science Centre, Abingdon, OX14 3DB, UK

1) Consorzio RFX (CNR, ENEA, INFN, Universita' di Padova, Acciaierie Venete SpA), Corso Stati Uniti 4, 35127 Padova, Italy.

2) Department of Industrial Engineering, University of Rome "Tor Vergata", via del Politecnico 1, Roma, Italy

3) National Institute for Laser, Plasma and Radiation Physics, Magurele-Bucharest, Romania,

4) European Commission, B-1049 Brussels, Belgium

5) Institute of Nuclear & Radiological Sciences and Technology, Energy & Safety, NCSR Demokritos, Athens 15310, Greece

6) Instituto de Plasmas e Fusão Nuclear, Instituto Superior Técnico, Lisbon, Portugal

Abstract

The next generation of Tokamak devices is expected to work at very high radiated fractions, well above 90%, to preserve the integrity of the plasma facing components in general and the divertor in particular. In addition to maintaining high confinement, these configurations will have also to guarantee a low disruptivity. An accurate determination of the emitted radiation will therefore become increasingly important, not only for the global power balances but also for specific regions of the plasma cross section (for example to properly control detachment). In this perspective, a new tomographic inversion method, based on the Maximum Likelihood approach, capable of providing routinely confidence intervals in the estimates of the radiated power, has been applied to the investigation of high radiative discharges on JET with the ITER Like Wall. The emission has been increased with injection of extrinsic impurities. Taking into account all the major sources of uncertainties, a systematic analysis of the configurations has shown that it has not been possible to develop stable configurations with radiated fraction higher than 70% of the input power. At higher radiated fractions the discharges always disrupt. Therefore a lot of work remains to be done to extend JET operation in a reactor relevant regime of sufficient radiation in preparation for ITER and DEMO.

Keywords: Total Radiation, Radiation limit, Tokamak, Tomography. Maximum Likelihood

Corresponding author: emmanuele.peluso@ uniroma2.it

*See the author list of E. Joffrin et al. accepted for publication in Nuclear Fusion Special issue 2019, https://doi.org/10.1088/1741-4326/ab2276

1 Tokamak Operation at high radiated power and tomography

In the next generation of Tokamak devices, stable and robust configurations at high radiated fraction, indicatively with radiated power above 90% of the input power, are indispensable to reduce the loads on the divertor plates to levels manageable by realistic types of materials. High radiation losses from the divertor and the SOL, enhanced by the injection of suitable extrinsic impurities, are a possible route, provided the accumulation of impurity in the core can be kept at manageable levels. Of course high radiation should neither affect confinement nor increase significantly the disruptivity of the configurations [1-3]. In the perspective of the reactor, high radiation scenarios should also preserve an adequate level of density peaking, to maximize the neutron yield. Investigations of high radiative configurations have therefore to address two main aspects: the thermal stability of plasma operation and the effects of radiation on confinement and neutron yield. The compatibility of safe and high performance plasma configurations with high radiated fraction is an important issue for the baseline scenario. It is even more crucial for advanced Tokamak and hybrid configurations, which have to implement a quite delicate control of the current profile.

On JET, since the installation of the new ILW (ILW), the two main impurities affecting the plasma behaviour are Be and W and typically, in discharges without extrinsic impurities, the total radiation is of the order of 30% of the input power. Therefore various experiments with impurity seeding, using N, Ne and Kr, have been performed to increase the radiated fraction. The database of specific experiments, carried out in JET with the new ITER Like Wall (ILW) injecting N, Ne and Kr, is overviewed in Section 3. Unfortunately it has proved to be very difficult to achieve stationary conditions with radiation above 70% of the input power. The attempts to exceed significantly this limit tend to destabilise the plasmas, which disrupt. The objective of this paper is to investigate the details of the emission and to start elucidating the mechanisms leading to the thermal instabilities and the subsequent disruptions. Of course in this perspective, a careful estimate of the radiated power, with associated confidence intervals, is an essential ingredient as discussed later in more detail.

In tokamaks devices, the total emission of radiation is measured with specific diagnostics called bolometers [4]. The bolometric diagnostic on JET is based on metal foil absorbers, which have a quite flat absorption coefficient in the wavelength regions of interest, the UV and SXR. These sensors integrate the radiation emitted along specific lines of sight (see next Section) and have been operated for many years, providing good quality measurements. On the other hand, to determine the total radiated power, the measured line integrals have to be processed with suitable tomographic inversion algorithms. One of the

main difficulties, in interpreting traditional tomographic techniques, resides in the fact that they do not naturally provide confidence intervals to be associated with their estimates. Therefore, particularly in the perspective of operation at high radiated fraction, a tomographic method capable of quantifying the uncertainties in the reconstructions on a routine basis would be very beneficial. An accurate estimate of the uncertainties is certainly essential when approaching high radiation fraction from both the point of view of the plasma control and interpretation of the physics. One of the main added values of the recently developed tomographic method, based on the Maximum Likelihood (Section 2), is precisely the quantification of the uncertainties in the radiated power, given the instrumental errors of the diagnostic (Section 4). This is the technique used for the analyses presented in the rest of the paper. The results for a series of experiments with impurity seeding on JET are reported in detail in Section 5 before drawing some conclusions in the last section of the paper.

2 Maximum Likelihood approach to Tomography

As mentioned, on JET the radiation emitted by the plasma is measured routinely with a tomographic system based on metal foil bolometers. The diagnostic comprises two cameras with horizontal and vertical views across the cross-section of the plasma. 24 chords are available for each view. The availability of basically only two views leads to a quite limited data set tomography. Given the layout of the diagnostic, reported in Figure 1, and the shape of the radiation emission (see Section 3 and 4), the tomographic inversion of the bolometric signals on JET is a very ill-posed problem. Therefore, to determine both the total radiated power and the local emissivity, quite sophisticated tomographic inversion methods are required. Special algorithms, specific to the machine and to its topology, and allowing effective tomography from the available limited data, are needed. In the course of the years, various tomographic methods have been tested [5-10] at JET. In order to converge on

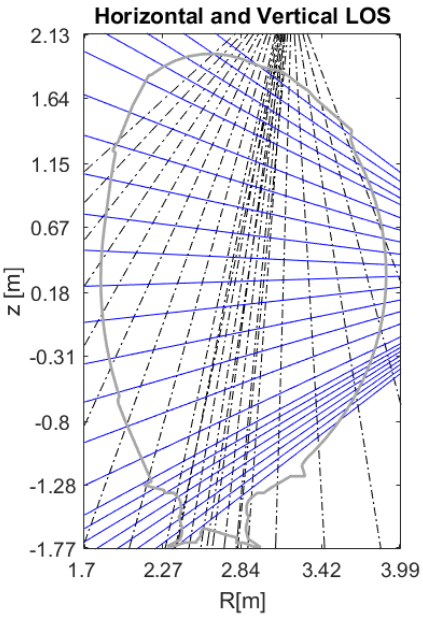

Figure 1 – Schematic view of JET bolometric diagnostic layout. Black dashed dotted lines: 24 lines of sight of the vertical camera. Blue continuous lines: 24 lines of sight of the horizontal camera.

physically meaningful solutions, all these techniques present the following two main characteristics: they make use of the prior information about the magnetic topology and implement more or less sophisticated forms of regularization. Tomographic reconstructions are currently performed with a method which implements the discretization of the tomographic problem using a grid of pyramid local basis functions [5-6]. The algorithm searches for a solution, which is constant on flux surface and slowly varying in the radial direction. The Maximum Likelihood (ML) Tomography, used to obtain the results reported in this paper, utilizes the information about the magnetic topology as well but avoids the use of a cost function with a regularization term. Indeed the approach is based on imposing a constraint on the pdf of the solutions and is implemented by a version of the Expectation Maximization algorithm, more robust against violation of the hypotheses about the statistics and the form of the emission [10].

In mathematical terms, the tomographic reconstruction of 2-D emission from integrated lines of sight, called projections, can be formulated in matrix form as:

$$g = Hf + n_g \qquad (1)$$

where g is the vector of the experimental measurements, f denotes the local emissivity and n_g is the zero mean noise of Gaussian distribution. The measurements are spatial integrals over the emissivity distribution, taken along physically well-defined lines of sight. The projection matrix element H_{mn} represents the probability of detecting the emission from pixel n in projection m.

In the original formulation of the maximum likelihood method, it is assumed that the total emission is a Poisson process and therefore that the individual line integrals g_m are sampled from a Poisson distribution, whose expected value is $\bar{g}$. Therefore, it is possible to express the probability of obtaining the measurement $g = \{g_m | m = 1, \dots, N_d\}$ from the emissivity $f = \{f_n | n = 1, \dots, N_p\}$ with the following likelihood function:

$$L(g/f) = \prod_m \frac{1}{g_k!} (\bar{g})^{g_k} \times exp(\bar{g}) \qquad (2)$$

Consequently, instead of implementing a regularization term, the ill posed tomographic problem is constrained by imposing a Poisson statistics on the solutions [8-10]. This allows solving the inversion by an iterative procedure of the Expectation Maximization family.

Indeed, the ML estimate of the local emissivity is obtained by maximizing the above expression iteratively [8,11], implementing the relation:

$$f_n^{(k+1)} = \frac{f_n^{(k)}}{s_n} \sum_m \left(g_m / \sum_j H_{mj} f_j^{(k)} \right) H_{mn} \quad (3)$$

where k is the iteration index and $s_n = \sum_m H_{mn}$ is the probability that a photon originating in pixel n is recorded.

In the present work, the derivation of approximate equations for the mean and uncertainties of the reconstructions is based on the general formalism developed in [8-9].A preconditioned gradient ascent algorithm has been implemented for solving (3), which, under very reasonable assumptions, allows calculating independently the local emissivities and the associated uncertainties with two separate iterative formulas:

$$f^{(k+1)} = f^k diag\left[\hat{f}^{(k)}\right] diag[s^{-1}] \left[H^T diag\left[H\hat{f}^{(k)} \right]^{-1} g - H^T I \right)\Big] \quad (4)$$

$$\varepsilon^{(k+1)} = diag\left[\hat{f}^{(k)}\right] diag[s^{-1}] H^T diag\left[H\hat{f}^{(k)} \right]^{-1} n + \left[I - diag\left[\hat{f}^{(k)}\right] diag[s^{-1}] H^T diag\left[H\hat{f}^{(k)} \right]^{-1} H \right] \varepsilon^{(k)} \quad (5)$$

where ε^k indicates the uncertainty at iteration k. When the difference of the correlation coefficients, between two subsequent iterations of equation (4), becomes less than 1 %, the

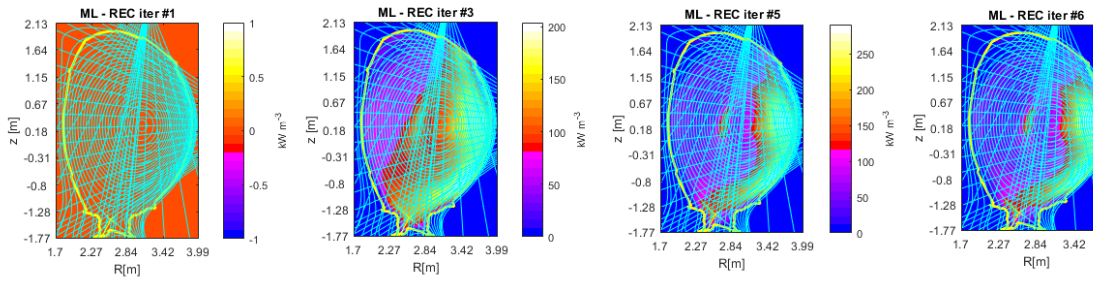

Figure 2 –Example of the iterations leading to the final estimate of the 2d emissivity using the ML algorithm.

algorithm is stopped. An example of some iterations, leading to convergence to the final

estimation of the radiation emission, is reported in Figure 2. As already discussed, on JET the bolometric tomography is a very ill-posed mathematical problem. To obtain realistic and robust solutions, it is therefore indispensable to introduce additional *a priori* information, in order to compensate for the lack of experimental evidence. A widely adopted approach consists of imposing smoothness of the solutions. The ML method developed for JET bolometric diagnostic incorporates a smoothing along the magnetic surfaces, given by the plasma equilibrium. Two different smoothing techniques, one for the closed and one for the open magnetic surfaces, have been implemented to better adapt JET bolometric tomography to the topology of the emission and the layout of the diagnostic. With regard to the closed magnetic surfaces, the smoothing is implemented as a 1-D average filtering, using a sliding window, which moves along the magnetic contour lines [10-12]:

$$f_i^{smooth}{}_i = \frac{1}{2 \cdot w_{ave}} \sum_{\substack{j=-w_{ave} \\ [-w_{ave}, w_{ave}] \in L_p}}^{w_{ave}} f_j \qquad (6)$$

where L_p designates the p-th close magnetic contour line, f^{smooth} is the emissivity after applying the smoothing and w_{ave} is half the width of the filtering window. For the open magnetic surfaces, to handle the fact that the field lines can be quite short, a smoothing spline procedure has been implemented, which is based on the minimisation of the expression:

$$p \sum_i \left(f_i^{smooth} - f_i\right)^2 + (1-p) \int (f_i'')^2 dx \qquad (7)$$

where f'' is the second derivative of f and $p \in (0,1)$ is an adjustable parameter. If p =0 the minimization of (7) consists of a least-squares straight-line fit to the data, while for p = 1 the interpolant is a cubic spline.

With reference to the application of the ML to the actual bolometric tomography on JET, a few clarifications are in point. First of all, the solution of equation (2) is obtained in practice with a procedure based on relation (3) and therefore implements an Expectation Maximization procedure (EM). It is well known, and widely reported in the literature, that the EM approach is not very sensitive to the details of the measurements distribution function [11, 12]. Therefore, even if the data and its uncertainties do not follow a Poisson distribution, the method converges anyway on valid solutions (with the penalty of some inefficiency). In any case, to further reassure the users of this fact, a systematic series of tests has been

performed with the method of the phantoms. A series of realistic emissivities, covering all the cases typically encountered on JET, have been generated and an appropriate level of noise has been added to the respective line integrals [13,14]. The reconstructions obtained with the ML approach not only reproduce the phantoms very well but the actual emitted power is always in the confidence intervals provided by the methodology [13,14]. An example, for a quite complex type of phantom, is reported in Figure 3. The reconstruction of this figure is noteworthy in two main respects. First, the actual emission within any flux surface is almost always well within the uncertainty band derived with the ML method. Moreover, the total emitted power at ψ =1 is very close to the actual estimate of the ML method. These two properties are very important and they are absolutely general aspects of all the reconstructions of the emissivities investigated in this paper.

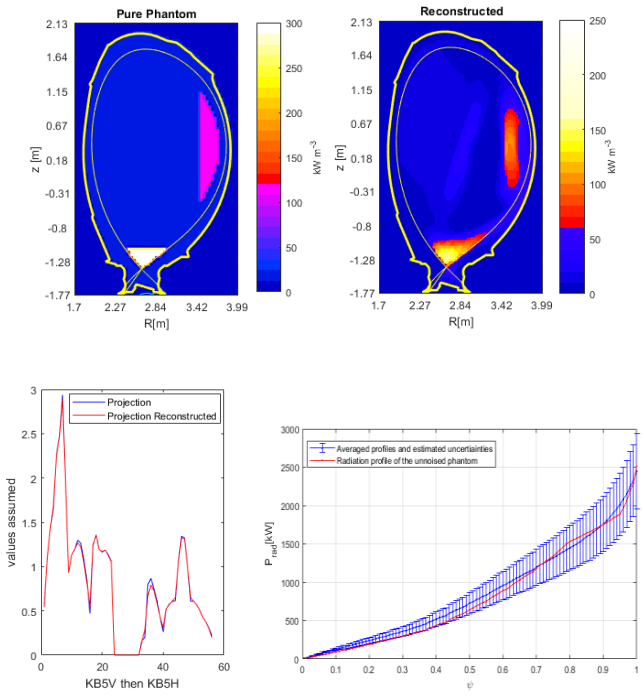

Figure 3 –Tomographic reconstruction of a complex phantom with two features: a strong emission region above the X point and a blob in the outer midplane. This topology of the emission is certainly more complex than most of the experimental cases analysed in the paper. Top left: phantom. Top right: reconstruction. Bottom left: comparison of original and reconstructed lines of sight. Bottom right: on the y axis the power emitted within the flux surface reported on the x axis.

In terms of computational time, for the parameters of the reconstructions chosen for the studies performed in this work (see next section), the CPU time is about I minute for each time slice, using a single core computer. Since the reconstruction of each time slice is independent from the others, the ML tomographic algorithms are fully parallelizable and therefore, with a reasonable amount of cores, a quite detailed analysis of the emissivity and the uncertainties can be performed between shots.

3 The database, the seeding schemes and the parametrization of radiation

On JET with the ILW, the main impurities used for seeding, to increase the radiated fraction, are N, Ne and Kr. The experiments analysed in this work were mainly discharges at 2.5MA/2.6T with the strike points on the vertical targets. The input power, most from the neutral beams, ranged between 17 MW and 19 MW. A few MW of ICRH were typically injected to avoid impurity accumulation in the core. The impurity seeding was performed with valves injecting in the divertor private region. Deuterium was fuelled by valves located on the divertor vertical targets. The overall database consists of 54 H mode baseline discharges: 31 with N seeding, 13 with Ne seeding and 10 with Kr seeding. The list if discharges, including the impurity rate and the divertor status (detachment or attachment), is provided in Appendix A. With regard to the evolution of the plasma in the divertor, detachment, when it occurs, takes place typically well in advance of the disruption time and normally early after the beginning of the impurity seeding.

The tomographic tools described in Section 2 allow a detailed spatial analysis of the emissivity. On the other hand, it is also important to aggregate the emission of the pixels belonging to specific and important regions, to provide a concise characterization of the type of radiation emission. To this end, the following four quantities have been calculated. The "core radiation" (P_{core}) is defined as the one emitted inside the separatrix. The "emission in the divertor" (P_{div}) is calculated as the radiation emitted for the Z coordinate below the one of the X point. The total radiation emission minus the sum of the radiation in the divertor and in the core is considered belonging to the SOL (P_{sol}). These are traditional definitions already established in the literature. To address the issue of thermal stability, a new region has been introduced, which consists of a horizontal band inside the separatrix between the Z of the X point and the Z coordinate Z=-0.8; this will be referred to as "radiation above the X point" (P_z) in the rest of the paper. A simple visualization of these regions is provided in Figure 4. It is worth mentioning that it has been checked, again with

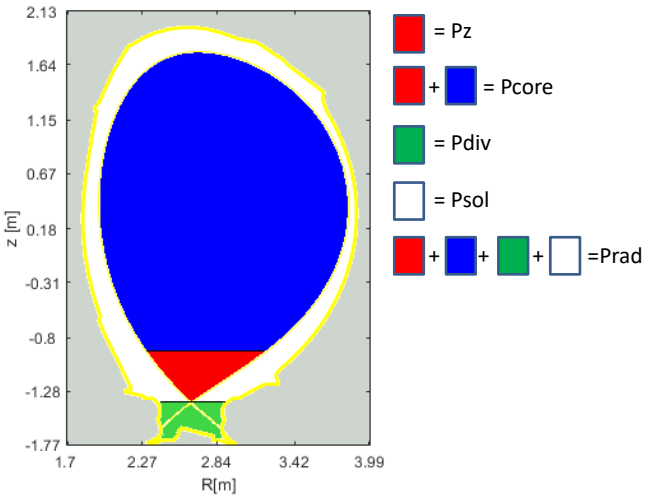

Figure 4 –Pictorial view of the emitting regions considered in this paper.

the method of the phantoms, that the ML method can properly estimate the emissivities and their uncertainties in all these regions of the plasma cross-section [13,15].

4 Assessment of uncertainties

As already briefly discussed, the specificity of the tomographic inversion with the ML approach consists of the capability to provide a reliable and fast estimate of the uncertainties in the reconstructions. This aspect has been extensively investigated with a series of numerical tests with phantoms [13,14]. In this section, examples are shown to illustrate the methodology adopted to determine the proper level of uncertainties in the final emissivities, as a function of the errors in the measurements. The impact of random errors is addressed in subsection 4.1 and the repercussions of the systematic errors, particularly in the equilibrium, are discussed in subsection 4.2.

4.1 Effects of the instrumental noise

The level of instrumental noise is an important input for the calculation of the uncertainties in the final reconstructions, obtained from equation (5). The systematic errors due to the acquisition system are taken into account in the calculations reported in the following but they constitute a marginal source of uncertainty. In reality, the measurements are dominated by the statistical noise, which in turn depends on the integration time. For the analyses reported in this paper, the random noise has therefore been calculated as the standard deviation of the projection signals over the integration time. Given the fact that JET

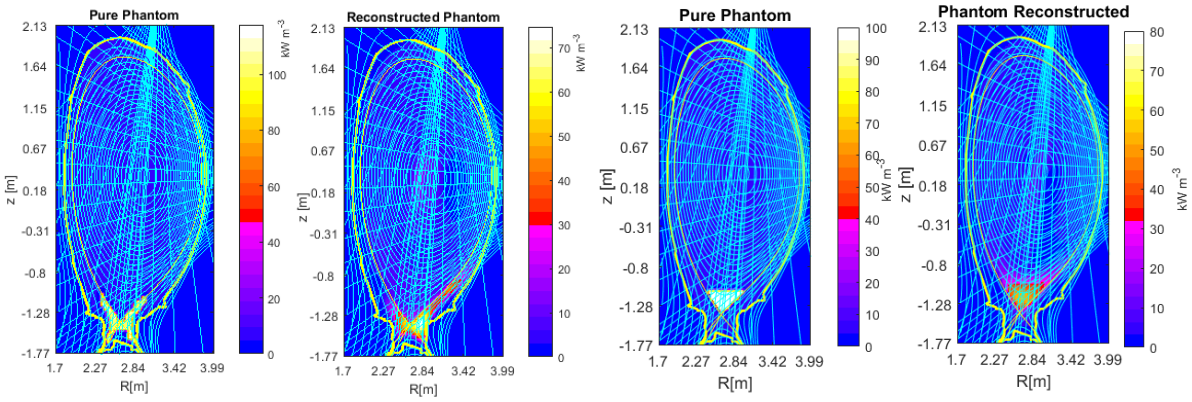

Figure 5 –Phantoms reconstructions for some of the most common types of emissivities on JET. The level of noise added to generate the phantoms is 10% of the line integrals, a value certainly representative of the experimental situations encountered in practice.

bolometry has a sampling time of 0.2 ms and the integration time chosen in this paper is 25 ms, the standard deviation has been calculated using 125 values. Since the bolometric sensors are integrators and therefore a derivative is necessary to obtain the instantaneous power, the measurements of the line integrals are quite vulnerable to noise spikes. The signals have therefore been properly cleaned by eliminating both negative values and spurious positive outliers [14]. To identify the last ones, for each LOS the scaled median absolute deviation of the measurements has been calculated to quantify the variability of the data in each time window. Measurements, which exceed three times this value, are therefore considered as potential outliers, unless they are consecutive and last for longer than 1ms. It has been double-checked that, with this filtering algorithm, only relevant physical measurements are retained in the averages [14].

To test the sensitivity of the reconstruction method to the random noise in the measurements, a systematic analysis based on a set of phantoms, representative of the main types of emission encountered in JET, has been performed [8,13,14]. A couple of examples are reported in Figure 5, for two types of emissivity among the most relevant for the investigations subject of this paper. The noise level implemented for the case in the figure is 10 % of the actual line integrals and is representative of all the most common radiative patterns encountered on JET, as analysed in detail in [14]. The effects of the noise typically do not result in an uncertainty higher than 10 % in the final reconstructions. More importantly for the purpose of this work, for all the phantoms tested the correct value of the radiated power is always included in the range of uncertainties estimated with equation (5). Therefore the values provided by this

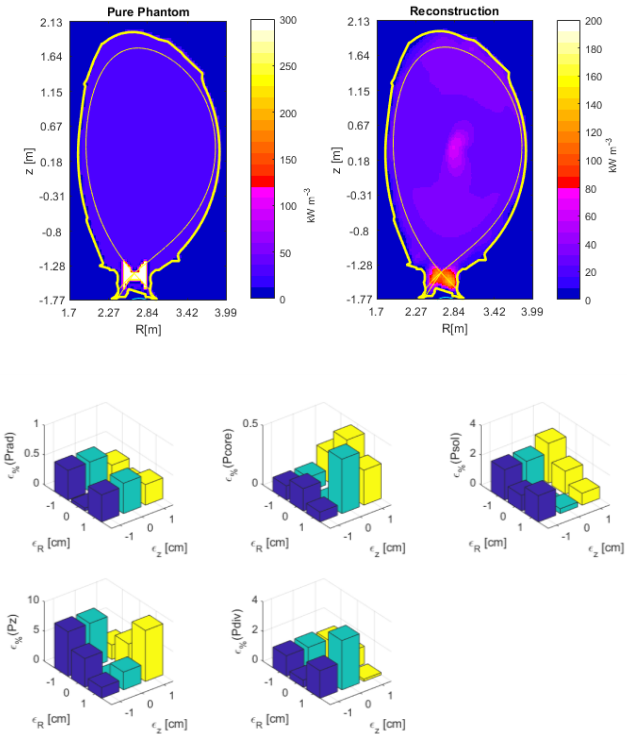

Figure 6 – Top left: Original phantom. Top right: reconstruction with the ML method. Bottom Additional error in percentage of the radiation in the various regions. The addiitonal error is due to the shift of 1cm left and right of the phantom above.The aforementioned shift is meant to simulate an error in the magnetic topology.

equation are a sort of maximum level of the uncertainties. Moreover, as already mentioned in Section 2, the estimated power, the centre of the confidence intervals, is typically very close to the actual value of the phantom emission and can therefore be considered a good estimate of the radiation, at least in the first approximation (see for example Figure 3).

4.2 Effects of uncertainties in the equilibrium

As mentioned, the layout of the bolometric diagnostic on JET is such that the tomographic inversion is a very ill-posed problem. To obtain reasonable results, it is therefore indispensable to profit from the information about the magnetic topology. Unfortunately, the identification of the magnetic equilibrium is another ill-posed problem and therefore also the magnetic reconstructions have uncertainties [15,16]. On the other hand, the calculation of the uncertainties in the tomographic reconstructions, with the iterative formula (5), considers only the propagation of the instrumental errors in the inversion process. The systematic uncertainties due to the imprecisions in the reconstructions of the magnetic topology are not taken into account. To our knowledge this aspect has been properly assessed only very recently at least on JET [14]. To investigate this additional source of uncertainty, the magnetic topology has been subjected to a rigid shift of ±1 cm in both the vertical and horizontal direction. Such an error in the magnetic topology is to be considered realistic given the quality of the equilibrium reconstructions on JET. This test has been applied to all the main radiative patterns. The final additional uncertainties are typically of the order of few per cent of the total radiated power. Higher errors have been found only in some "pathological cases", when a very high radiation is emitted by features located exactly at the border between different regions. Therefore it can be concluded that the effects of the errors in the equilibrium reconstructions do not contribute significantly to the uncertainties in the estimates of the radiated power with the maximum likelihood method. To illustrate the basis for this conclusion, Figure 6 reports a case for a phantom meant to simulate one of the most important experimental radiation patterns. This case is representative of the other main typologies of emissivity analysed in this paper.

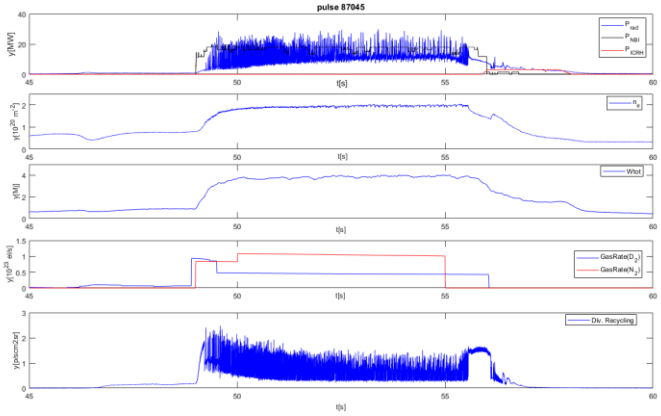

Figure 7 –Typical discharge with N seeding.

5 Evolution of total radiation emission leading to disruptions

In this section, evidence of the total radiation evolution leading to disruptions is shown in detail. The phenomenology is very similar for Nitrogen and Neon (see subsection 5.1 and 5.2) but completely different for Krypton (see subsection 5.3).

5.1 Nitrogen seeding

Nitrogen is probably the most widely investigated impurity for seeding on JET. Various discharges with a quite stable flat top phase have been obtained at different levels of input power and seeding. An example is shown in Figure 7. Since the influx of high impurities is a major problem for JET with the ILW, the traditional recipe of high deuterium fuelling before the switching on of the neutral beam was adopted. In the experiments investigated in this paper, the seeding was started typically 100 ms after the NBI heating was switched on.

A total radiated fraction of about 70% was achieved quite reliably with this scheme. These discharges present about 30% of radiated fraction without seeding. Crossing this level of 70% of radiation, the thermal stability is affected and the discharges terminate with a disruption. The phenomenology leading to the disruption is typically the one shown in Figure 8; a higher level of radiation is emitted above the X point within the separatrix instead of in the divertor. Excessive radiation from this region seems to be the cause of the disruption. This behaviour is common also to Ne as shown in the next subsection (discharges with Kr seeding present a different behaviour as discussed later).

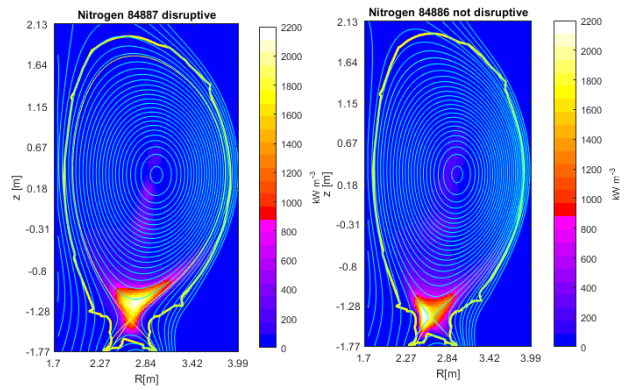

Figure 8 –N seeded discharge. Left: 50 ms before the beginning of the current quench. Right: 500 ms before the beginning of the current quench.

5.2 Ne seeding

In terms of global parameters, the results obtained with Ne and N are very similar. Also the distribution of the emission in the five regions defined in Section 3 is very similar and does not differ outside the uncertainties in the reconstructions. The dynamics of the radiation leading to disruptions is also analogous; increasing the seeding the maximum radiation starts being emitted in the region above the X point instead of in the divertor. In the

case of Neon, a clear threshold can be seen in the emission above the divertor (see Figure 9). When the radiated fraction emitted in this region exceeds about 10% of the input power, the plasmas disrupt. A similar threshold can be identified also for N but at higher values, around 15%. As can be easily appreciated from inspection of Figure 9, in the other regions there is not clear threshold separating the disruptive from the safe cases. These plots are also representative of the radiation patterns in N. For these impurities (N, Ne), it is therefore reasonable to assume that the radiation in the region above the divertor is the critical factor leading to disruptions.

5.3 Kr seeding

The discharges with Kr seeding present a quite different phenomenology than the others. The radiation pattern in the phase preceding the thermal quench is quite different. A representative situation is reported in Figure 10, from which it can be appreciated how the

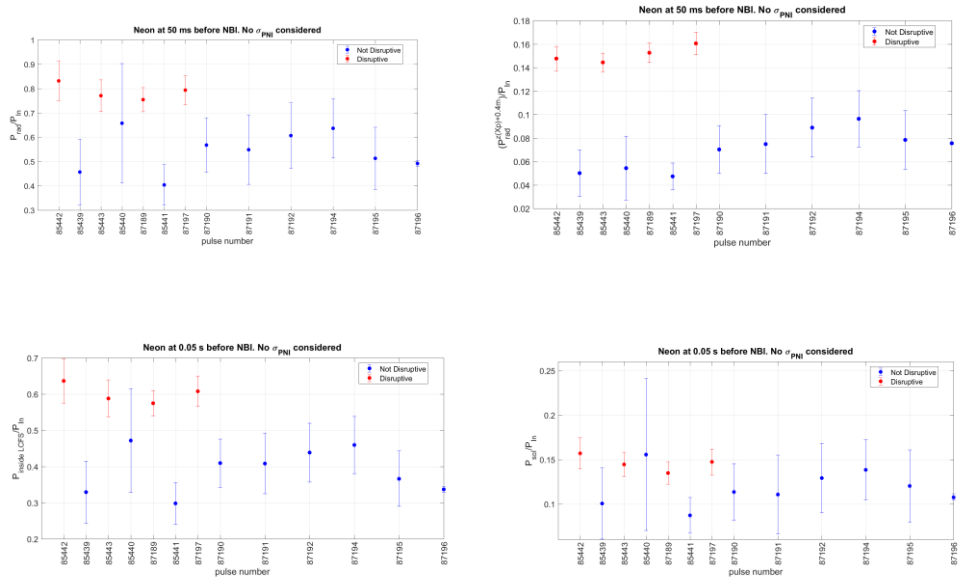

Figure 9 –Neon seeding. Radiated fractions in the various zones at 50 ms before the beginning of the current quench. Top left: total radiated fraction. Top right: radiated fraction above the X point. Bottom left: radiated fraction within the LCMS. Bottom right: radiated fraction in the SOL.

radiation emitted above the X point is quite small. On the other hand, the radiated fraction in the core is higher and seems to be the cause of the collapse of the configuration. Indeed, the plots reported in Figure 11, analogous to those for Neon, show how a clear separation between the disruptive and safe discharges can be seen most clearly now in the radiated fraction emitted within the LCMS. When the radiation in this region exceeds about 60% of

the input power, the discharges disrupt. On the other hand, there is no clear demarcation in the radiation above the X point, which seems to be the critical quantity for seeding with N and Ne. The maximum radiated power achieved with Kr is lower than the one reached with the lighter impurities, since non disruptive configurations with radiated fraction higher than 60% have not been achieved.

The distinctive feature of the case of Kr is the concentration of the emission in the equatorial plane. This is a consequence of the centrifugal forces resulting from the high toroidal rotations of these plasmas, of the order of tens of km per second. The emitted power density (per unit volume) is clearly lower (about a third) than in the case of the MARFE above the divertor. On the other hand the volume is quite comparable. It should also be mentioned that

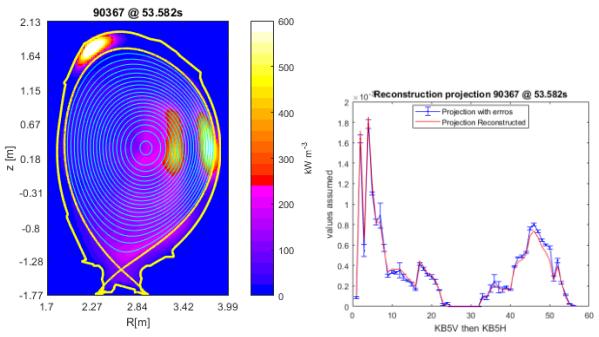

Figure 10 –Kr seeded discharge. Left: emissivity 50 ms before the beginning of the current quench. Right: comparison between the measurements and the reconstructed projections.

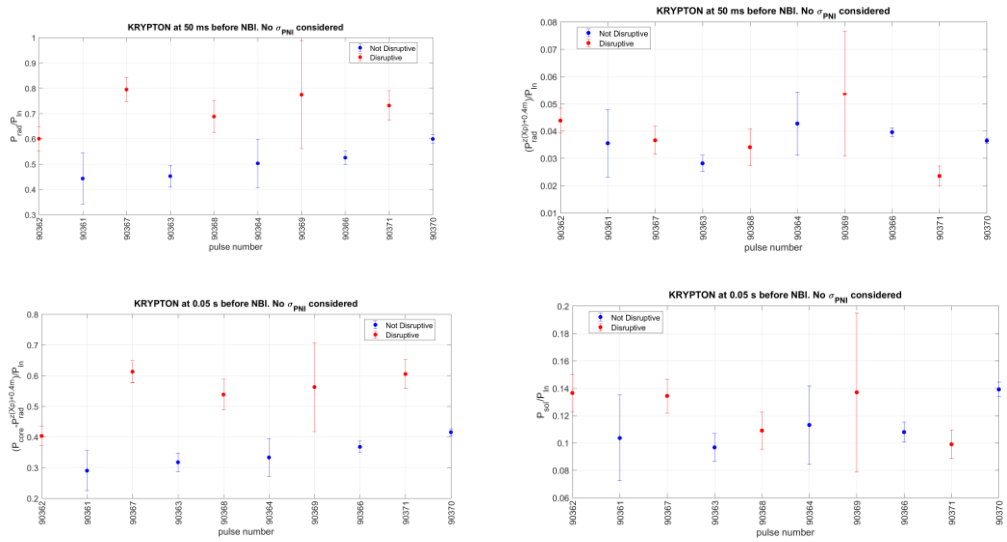

Figure 10 –Kr seeding. Radiated fractions in the various zones at 50 ms before the beginning of the current quench. Top left: total radiated fraction. Top right: radiated fraction above he X point. Bottom left: radiated fraction within the LCMS. Bottom right: radiated fraction in the SOL.

the blob of high radiation in the upperpart of the machines (see figure 10) is real and not an artefact. This region is indeed known to be a stagnation point for the flow in the SOL.

6 Summary and conclusions

In this paper, the main aspects of a relatively new tomographic reconstruction method, based on the maximum likelihood, have been presented. Specific attention has been accorded to the competitive advantages of the approach, in particular the routine estimation of the uncertainties. The technique has been applied to the investigation of the total radiation in JET, using the line integrals of the bolometric diagnostic. A series of discharges with impurity seeding, devoted to the investigation of high radiated fraction regimes, has been analysed in detail, with the aim of investigating the thermal stability of the configurations. In global terms, disruptions typically occur for the highest levels of impurity seeding. On the other hand, no clear elation with the detachment has been detected. Indeed it is not only the case that discharges with both detached and detached divertor can disrupt but also that the detachment typically takes place very early in the discharge (even seconds before the beginning of the current quench).

The evolution of the radiation leading to the disruption is different depending on the impurity use for the seeding. N and Ne show very similar behaviour, with the radiation increasing in the region above the X point and causing a radiate collapse for radiated fractions above 70%. For the discharges with these impurities, the critical zone seems therefore to be the one above the divertor, where a MARFE type of radiative blob typically forms before the disruption. On the contrary, seeding with Kr tends to show increased radiation in the outer equatorial plane, which can destabilise the configuration even before the maximum of the radiation reaches the very centre of the plasma. Again the tomographic reconstructions indicate that the threshold in the power fraction is again of the order of 70%. It should be mentioned that, even if one considers the maximum of the confidence intervals in the estimates of the total power and not the most likely value, practically no stable discharges with radiated fraction of 90% or higher have ever been run. So even in the most optimistic and probably unjustified interpretation of the tomographic results, the configurations developed so far do not meet ITER requirements in terms of thermal stability. This observations applies also to the confinement, since the H factor is always well below 1 in these discharges.

With regard to future developments, the tomography based on the maximum likelihood is expected to provide valuable information for the evaluation of the energy balances on JET. In this perspective, it is worth mentioning that the radiated fractions reported in the paper have been calculated using the nominal value of the deposited power by the neutral beams.

On the other hand, various studies, published in the past [18,19] and based on tile thermocouples, seem to indicate that typically about 25% of total input remains unexplained. The numerous investigations performed so far suggest that the missing energy varies collinearly with the neutral beam injection heating (NBI). This has motivated a detailed analysis of the NBI injected energy, resulting in the hypothesis that the NBI power might be overestimated by about 10%. This would increase the maximum radiated fraction of the same amount, 10 %, for all the cases reported in the paper. On the other hand, the results of the ML tomography basically confirm the estimates of the total radiated power used in the past for the energy balances and therefore there is still a significant amount of input energy unaccounted for in the losses.

The maximum likelihood tomography could provide interesting information also for more advanced studies. For examples it seems to be a very good candidate for the investigation of the confinement in high radiative discharges. In addition to its accuracy and versatility, the proper assessment of the uncertainties is an important aspect also for the investigations of the effect of high radiation on transport and for the experiments which require a carefull tailoring of the current profile [20].

Aknowledgements

This work has been carried out within the framework of the EUROfusion Consortium and has received funding from the Euratom research and training programme 2014-2018 and 2019-2020 under grant agreement No 633053. The views and opinions expressed herein do not necessarily reflect those of the European Commission. This work was also partially funded by the Spanish Ministry of Economy and Competitiveness under the Project No. ENE2015-64914-C3-1-R

References

[1] Lowry C.G. European Fusion Physics Workshop, Ericeira, Portugal, 3-5 December 2012
[2] Wischmeier M. et al Journal of Nuclear Materials 415 S523-S529
[3] Martin Y.R. for the H-mode Power Threshold Working Group, Proceedings of the 20th IAEA Fusion Energy Conference, Vilamoura, Portugal, 1-6 November 2004
[4] A. Huber, K. McCormick, P. Andrew, P. Beaumont, S. Dalley, J. Fink, J.C. Fuchs, K. Fullard, W. Fundamenski, L.C. Ingesson, F. Mast, S. Jachmich, G.F. Matthews, Ph. Mertens, V. Philipps, R.A. Pitts, S. Sanders, W. Zeidner, Upgraded Bolometer System on JET for Improved Radiation Measurements, Fus. Eng. Design 82-5 (2007) 1327-1334.
[5] L. C. Ingesson, B. Alper, B. J. Peterson & J.-C. Vallet (2008) Chapter 7: Tomography Diagnostics: Bolometry and Soft-X-Ray Detection, Fusion Science and Technology, 53:2, 528-576.
[6] L. C. Ingesson, B. Alper, H. Chen, A. W. Edwards, G. C. Fehmers, J. C. Fuchs, R. Giannella, R. D. Gill, L. Lauro-Taroni, and M. Romanelli, “Soft x-ray tomography during ELMs and impurity injection in JET,” Nucl. Fusion 38, (1998) 1675–1694.
[7] F. A. Matos, D. R. Ferreira, and P. J. Carvalho, “Deep learning for plasma tomography using the

bolometer system at JET," Fusion Eng. Des. 114 (2017) 18–25.
[8] T. Craciunescu, E. Peluso, A. Murari, M. Gelfusa, Maximum likelihood bolometric tomography for the determination of the uncertainties in the radiation emission on JET TOKAMAK, Rev. Sci. Instrum. 89 (2018) 053504.
[9] T. Craciunescu , A. Murari, V. Kiptily, I. Lupelli, A. Fernandes , S. Sharapov, I. Tiseanu, V. Zoita, Evaluation of reconstruction errors and identification of artefacts for JET gamma and neutron tomography, Rev. Sci. Instrum. 87 (2016) 013502.
[10] J. Mlynar, T. Craciunescu, D.R. Ferreira, D.R., P. Carvalho, O. Ficker, O. Grover, M. Imrisek, J. Svoboda, J. Fusion Energy (2018). https://doi.org/10.1007/s10894-018-0178-x
[11] Barrett H. H et al ,"Noise properties of the EM algorithm. I. Theory," Phys. Med. Biol. 39, 833–846 (1994).
[12] E. J. Soares, J. Glick, J.W. Hoppin, "Noise characterization of block iterative reconstruction algorithms: I. Theory," IEEE Trans. Med. Imaging, 19 (2000) 261–270
[13] E. Peluso, T. Craciunescu, M. Gelfusa, A. Murari, P. J. Carvalho, P. Gaudio, On the effects of missing chords and systematic errors on a new tomographic method for JET bolometry, Fus. Eng. Des., in press, https://doi.org/10.1016/j.fusengdes.2019.03.120.
[14] E. Peluso , T. Craciunescu, A. Murari, P. Carvalho, M. Gelfusa, A Comprehensive Study of the Uncertainties in Bolometric Tomography on JET using the Maximum Likelihood Method, submitted to Rev. Sci. Instrum.
[15] Gelfusa M. et al. Review of Scientific Instruments, Volume 84, Issue 10, October 2013, Article number 103508
[16] Murari, A., et al (2014) Review of Scientific Instruments, 85 (12), art. no. 123507, DOI: 10.1063/1.4904450
[17] Murari, A. et al Plasma Physics and Controlled Fusion, 54 (10), (2012) DOI: 10.1088/0741-3335/54/10/105005
[18] Matthews G.F. et al Phys. Scr. T170 (2017) 014035 (6pp), doi.org/10.1088/1402-4896/aa8de7
[19] Matthews G.F. et al 2016 Nucl. Mater. Energy (doi.org/10.1016/j.nme.2016.12.012)
[20] Mazon, D. et al Plasma Physics and Controlled Fusion, Volume 45, Issue 7, July 2003, Pages L47-L54

Appendix A. Overview of the seeded discharges.

Nitrogen					
Disruptive discharges			Safe discharges		
Pulse	State	~Imp. Rate (el/s)	Pulse	State	~Imp. Rate (el/s)
84885	detached	1.00E+23	84888	detached	7.00E+22
84887	detached	5.00E+22	85060	non-detached	5.00E+22
85067	detached	1.20E+23	85061	non-detached	6.00E+22
85427	detached	1.00E+23	87201	detached	1.60E+23
87051	detached	1.20E+23	91993	non-detached	1.00E+23
87198	detached	1.20E+23	91994	detached	1.00E+23
87202	detached	1.40E+23			
87496	detached	1.40E+23			
91990	detached	1.00E+23			
Safe discharges					
Pulse	State	~Imp. Rate (el/s)	Pulse	State	~Imp. Rate (el/s)
84886	detached	5.00E+22	87045	detached (shortly)	1.00E+23
84889	detached	7.00E+22	87046	detached (shortly)	1.00E+23
85059	non-detached	4.00E+22	87048	detached (shortly)	1.00E+23
85064	non-detached	6.00E+22	87199	non-detached	1.00E+23
85065	detached	6.00E+22	87200	detached (very shortly)	1.00E+23
85066	non-detached	4.00E+22	87497	non-detached	1.00E+23
85423	non-detached	6.00E+22	91989	non-detached	8.00E+22
85425	detached(shortly)	1.00E+23	91992	non-detached	8.00E+22

Neon					
Disruptive discharges			Safe discharges		
Pulse	State	~Imp. Rate (el/s)	Pulse	State	~Imp. Rate (el/s)
85442	non-detached	1.40E+22	85440	detached (shortly)	3.00E+20
85443	non-detached	1.20E+22			
87189	non-detached	2.00E+22			
87197	non-detached	1.20E+22			
Safe discharges					
Pulse	State	~Imp. Rate (el/s)	Pulse	State	~Imp. Rate (el/s)
87196	non-detached	6.00E+21	87191	non-detached	5.00E+21
87195	non-detached	3.00E+21	87190	non-detached	5.00E+21
87194	non-detached	1.00E+22	85441	intermitent detachment	1.00E+22
87192	non-detached	1.00E+22	85439	non-detached	6.00E+21

Krypton					
Disruptive discharges			Safe discharges		
Pulse	State	~Imp. Rate (el/s)	Pulse	State	~Imp. Rate (el/s)
90362	non-detached	1.20E+22			
90367	non-detached	3.00E+22			
90368	non-detached	1.50E+22			
90369	non-detached	1.40E+22			
90371	non-detached	1.60E+22			
Safe discharges					
Pulse	State	~Imp. Rate (el/s)	Pulse	State	~Imp. Rate (el/s)
90361	non-detached	1.00E+21			
90363	non-detached	1.00E+21			
90364	non-detached	1.50E+22			
90366	non-detached	1.50E+22			
90370	non-detached	1.50E+22			